PFC/RR-86-5 DOE/PC-70512-5

Develop and Test an Internally Cooled, Cabled Superconductor (ICCS) for Large Scale MHD Magnets

Analysis Report

Hatch, A.M., Marston, P.G., Tarrh, J.M.,
Becker, H., Dawson, A.M., Minervini, J.V.

January 1986

Plasma Fusion Center
Massachusetts Institute of Technology
Cambridge, Massachusetts 02139 USA

This work was supported by the U.S. Department of Energy, Pittsburgh Energy Technology Center, Pittsburgh, PA 15236 under Contract No. DE-AC22-84PC70512.

NOTICE

Table of Contents

List of Figures

List of Tables

1.0 Introduction

A three-year program to develop and test an internally-cooled cabled superconductor (ICCS) for large-scale MHD magnets is being performed by MIT for the Pittsburgh Energy Technology Center (PETC) under contract DE-AC22-84PC70512.

The program consists of the following four tasks:

I. Design Requirements Definition

II. Analysis

III. Experiment

IV. Full Scale Test

This report describes the analysis performed (Task II) in the period from the start of the program on August 21, 1984 through December 1985. It represents a progress report. Analysis is an ongoing effort which will continue in support of the testing, Tasks III and IV, and will be reported on again in the future.

Included in this report are electromagnetic, thermodynamic, structural, protection, and systems analyses, completed as required to substantiate the preliminary conductor design requirements definition and the associated preconceptual magnet design developed in Task I. (It was necessary to generate the design for a retrofit-size MHD magnet as a basis for establishing the characteristics and design requirements for the conductor.) Magnet and conductor designs are largely interdependent, and it was therefore appropriate to develop them in parallel. The magnet design could not be fully substantiated until after the conductor was defined.

Not included are analyses required to establish limits for conductor internal flow resistance and length between vents, and to support small-scale test conductor design, test equipment designs, and test plans. This work, not accomplished as of the date of this report, will be covered in a future report.

Copper-stabilized NbTi superconductor was selected at the outset as being most suitable for the application because

1. this superconductor has adequate current-carrying capacity at the magnetic fields required in magnets for linear MHD generators (4 to 8 T),
2. is easier and less expensive to manufacture and fabricate into coils than alternative superconductors such as Nb_3Sn, and
3. represents the commercially-available superconductor for which the greatest backgound of experience exists.

2.0 Summary

2.1 Magnet Analysis Summary

The analysis necessary to substantiate the preconceptual MHD magnet design is complete, including field and force calculations, preliminary structural analysis, thermodynamic (cryogenic) analysis, and the analysis of the magnet electrical and protective systems.

A significant result of the field analysis is the determination that maximum fields to which the conductor is exposed in the magnet are considerably higher than originally expected. At the start

of the program, it was estimated that maximum field for the conductor would be about 6 T, 33% above the peak on-axis field of the magnet. This relationship was consistent with the characteristics of existing MHD designs using bath-cooled conductor. However, when the initial ICCS winding design was analysed, maximum field was found to be 7.6 T (69% above central field) making the design unacceptable from the standpoint of stability. The high maximum field came about because of the relatively high winding current density achievable with ICCS, a feature advantageous in reducing magnet size and cost, but also resulting in the higher maximum-field-to-central-field ratio inherent with thin windings.

Changes were made to produce a revised design in which the maximum field is 6.9 T (53% above central field) and adequate stability is ensured.

The impact of the analysis and design revisions on conductor requirements is to reduce design current and current density by about 25% from initial values. The revised conductor and winding current densities are still substantially higher than those of magnet designs incorporating bath-cooled conductor.

The preconceptual magnet design is described in a Technical Progress Report.[1] The analysis done in support of the magnet preconceptual design is described in Section 3.1 of this report.

2.2 Conductor Analysis Summary

Analysis necessary to substantiate a preliminary conductor design requirement definition for full-scale conductor has been completed except that further work is required to establish maximum allowable internal flow resistance and maximum length between vents. Procedures for accomplishing these analyses have already been developed at MIT and by other contractors.[5]

Structural behavior of the full-scale conductor has been examined, based on exploratory tests previously performed.[2] Thermodynamic analysis has been performed on several alternative conductor designs to determine stability and quench heating characteristics, together with the analysis of pressure dynamics and of conductor heating under magnet emergency discharge conditions. Stressful conditions are imposed on the conductor both by the high internal pressure caused by quench heating and by the high temperature caused by emergency discharge. It was necessary, therefore to analyse these effects for all candidate conductors.

Further conductor analysis is required to finalize specific design parameters such as the copper-to-superconductor ratio, stability margin, and quench heating temperature rise. This analysis must be sequenced subsequent to the test results obtained under Tasks III and IV.

A listing of conductor design requirements in preliminary form is contained in the Design Requirements Definition Report.[3] The design requirements definition will be finalized upon completion of the conductor analysis and tests.

The definition and design of the experimental setup for conductor testing, including predictive analysis, will be initiated in the next period.

Analysis accomplished to date in support of conductor design requirements is described in Section 3.2 of this report.

3.0 Analysis

The analysis performed to substantiate both the preconceptual magnet design and the conductor design requirements definition is described below.

3.1 Magnet System Analysis

3.1.1 Electromagnetic Analysis

In order to perform the electromagnetic analysis, it was recognized that detailed three-dimensional computer modeling would be required to determine adequately the basic magnetic parameters, including: field profile on axis, field distribution in the magnet bore (homogeneity), fringe magnetic fields, peak fields at the winding, and magnetic forces. The first step in the analysis was thus to select an appropriate configuration, and then to develop a computer model for this configuration. The configuration selected was a tapered rectangular saddle coil, having end turns at an angle to the symmetry plane between coils. A rectangular saddle coil configuration was selected because it allows the warm bore of the magnet to be rectangular in cross section (rather than square or round), thereby providing more effective use of the high field volume. The coil taper allows for insertion of a tapered channel, while providing the desired taper in magnetic field along the channel axis. The end turn configuration provides maximum access to the flow train at both ends of the magnet by allowing the cryostat end surfaces to slope inward toward the magnet bore.[1] A sketch of this configuration is given in Fig. 1, including all of the parameters necessary to define a specific case, as well as a coordinate system for reference. Each coil is modeled using an $n \times m$ matrix of filaments, with n filaments through the coil width w and m filaments through the coil height h, where a filament is a sequence of straight, finite-length current-carrying elements of negligible cross section which are linked together end to end to form a loop around the coil. For this configuration, 16 such straight elements are required to form a complete filament. In the actual coil design, a finite cross-section conductor will be wound to provide a continuous current path of many turns in series filling the same envelope as the array of closed loops used in the computer model. A listing of the computer program that was written to generate the required filamentary models, based on this configuration, is included as Appendix A. A typical model, generated using the program with $n \times m = 2 \times 5$, is shown in Fig. 2.

It was originally anticipated that the electromagnetic analysis would consist of a rather straightforward application of the modeling techniques that have been described. Thus for a given set of parameters (i.e., a fixed geometry), the computer model would be generated (such as that shown in Fig. 2) and the most basic characteristics determined (field profile for a current density appropriate to the conductor under development) using existing computer programs to analyze the model. The model parameters would then be adjusted, as necessary, to obtain a satisfactory, self-consistent set of design parameters.

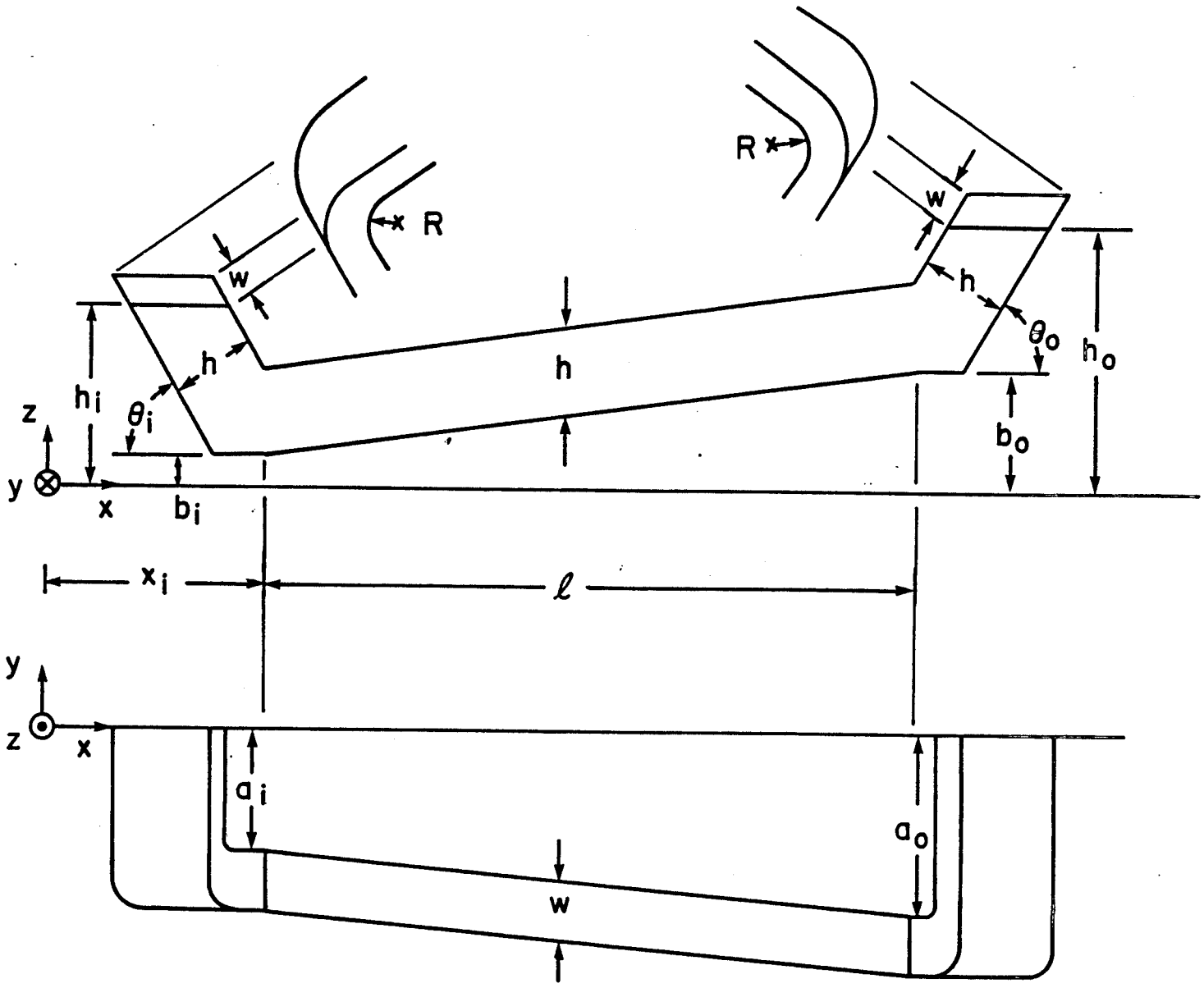

Fig. 1 Sketch of Tapered Rectangular Saddle MHD Coil with Ends at Arbitrary (Specified) Angles

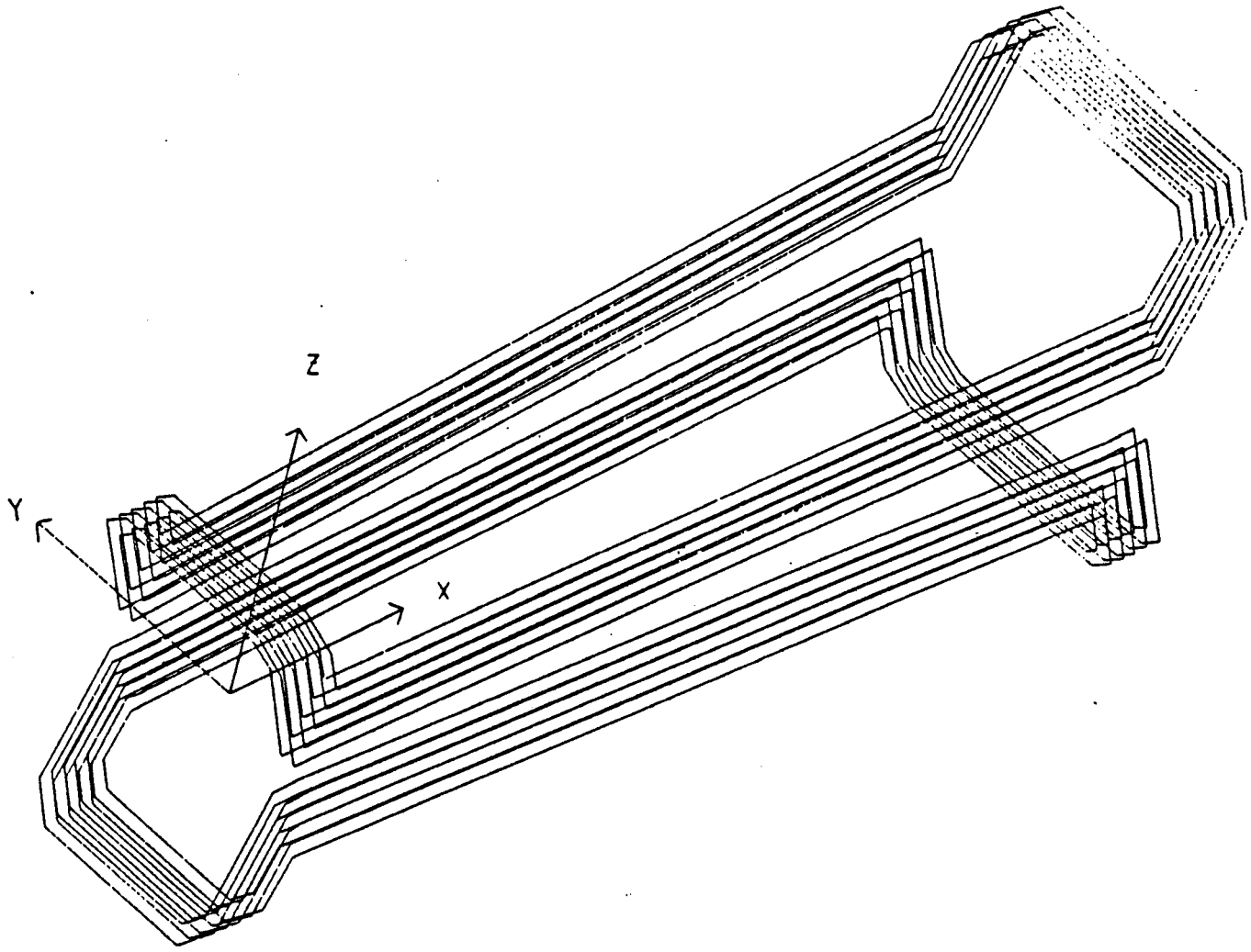

Fig. 2 Typical Computer Model for Electromagnetic Analysis, With n×m = 2×5

This process was performed without difficulty until the peak magnetic fields at the winding were first calculated. The peak field calculation is typically performed after the other parameters have been determined. Although the peak field value is extremely important in that it determines the maximum field to which the conductor will be exposed (and is therefore a critical parameter relative to conductor design and specification), it is a difficult and tedious calculation to perform. This is true because one must address the approximations inherent in the computer model relative to what the actual coil configuration would be, and then search throughout the model to locate the maximum field value at the winding. An effective approach is to assume a value for the ratio of the peak field at the winding to the maximum field on axis (based on experience with similar configurations), and use this assumed ratio to design the coil and conductor, and then verify that the actual peak field is acceptable.

The first detailed calculations of peak field at the windings gave results considerably higher than anticipated (approximately 7.6 T). This value of maximum field was incompatible with the planned conductor design, which was intended for use with a maximum field well below 7 T. To modify the conductor for operation in the higher field at the originally planned high current rating, more NbTi superconductor would need to be added, which in the fixed conductor envelope would result in removal of some of the copper and a significant reduction in the copper-to-superconductor ratio, which adversely affects stability.

NbTi has a relatively low critical field and hence its current-carrying capacity drops off rapidly at fields above 7 T. Calculations showed that it was impossible to achieve acceptable stability and safety margins without reducing the maximum field and/or the conductor current rating. It was clear that effort should be spent to determine how much reduction in maximum field could be achieved by modifying the coil configuration, after which tradeoffs would be made to arrive at a final set of characteristics (coil configuration, conductor current rating, maximum field and stability criteria) suitable for an early commercial magnet. In order to address this issue, the impact of various changes in the original configuration parameters on the peak field were examined by analyzing a number of different cases. The parameter values for four of these cases are listed in Table I. The parameters listed in the table correspond directly to those shown in the configuration sketch of Fig. 1 and to the list of input required for a particular case in the computer program listing of Appendix A.

Among these four cases, all of the currents were adjusted to achieve a maximum on-axis field of 4.5 T. Case I is the original configuration. Case II is similar to Case I, but with extended end turns and larger corner radii. Case III is similar to Case II, but with a 22% greater coil cross-sectional area, as well as a greater coil width-to-height ratio. Case IV is similar to Cases II and III, but with a 31% greater area than Case II (7.5% greater area than Case III) and an even larger width-to-height ratio than Case III.

The peak fields at the winding for the first two cases are approximately the same (7.2 T), although the location of the peak field for Case II is in the "straight section" (i.e., the long run of conductor rather than the end turns) whereas for Case I the peak field occurred both within the

end turns as well as within the straight section. For Cases III and IV, the peak fields at the winding are also approximately the same (6.9 T), and occur within their respective straight sections. A fifth case was also analyzed, consisting of 45° angles (rather than 60°) and carrying a current of 5.97 MA turns, but otherwise identical to Case IV. This case reduced the peak fields only slightly, to a value of 6.8 T.

The results of this analysis were then confirmed by comparison to a somewhat more fundamental, simplified approach. These results demonstrated conclusively that the only way to decrease the peak magnetic field at the winding to acceptable levels would be to decrease the winding current density and increase the coil cross section. Given this choice, a compromise of increasing the coil cross section (from Case I to Case III) was chosen, while accepting an increased peak field at the winding in the range of 6.8 to 6.9 T (in comparison to the originally assumed value of 6.0 T). This peak field increase impacted the conductor design by requiring a decrease in the current level for the same conductor cross section, as discussed in Section 3.2.2. The changes are actually self-consistent because increasing the coil cross section provides room for more turns of conductor, and when these extra turns are added, the design current in the conductor is automatically lowered to keep total ampere-turns at the required level.

The analysis of peak fields was a major result which significantly impacted the conductor design requirements. It should be noted, however, that the originally assumed ratio of peak field at the winding to maximum on-axis field, taken on the basis of earlier analyses and detailed calculations on larger, higher field magnets for base-load application, was confirmed by the present analysis. These higher-field magnets had substantially lower winding current densities and therefore much thicker windings. If the present analysis were applied to the earlier designs, peak-field-to-central-field ratios in the range of 1.33 would be obtained.

With the selection of Case III as the new baseline configuration, the electromagnetic analysis was completed with determination of the basic electromagnetic characteristics. These include the field profile on axis, field distribution in the magnet bore (homogeneity), and fringe magnetic fields. These results, as well as a diagram showing the location of the peak field at the windings and other high field points are given in a Technical Progress Report.[1]

The computer model described herein was also used to determine the magnetic forces on the windings. The results of this analysis are summarized in Figs. 3 and 4 and Table II in the following section.

Table I

CONFIGURATIONS ANALYZED FOR PEAK MAGNETIC FIELDS

Parameter	Case I	Case II	Case III	Case IV
Coil length between ends, l (m)	9.01	9.01	9.01	9.01
Coil width, w (m)	0.25	0.25	0.305	0.40
Coil height, h (m)	0.61	0.61	0.61	0.50
Bore half-width at inlet, a_i (m)	0.71	0.71	0.71	0.71
Bore half-width at outlet, a_o (m)	0.96	0.96	0.96	0.96
Coil half-gap at inlet, b_i (m)	0.08	0.08	0.08	0.08
Coil half-gap at outlet, b_o (m)	0.20	0.20	0.20	0.20
Crossover half-height at inlet, h_i (m)	1.00	1.13	1.13	1.13
Crossover half-height at outlet, h_o (m)	1.24	1.37	1.37	1.37
Inlet end turn angle, θ_i (°)	60	60	60	60
Outlet end turn angle, θ_o (°)	60	60	60	60
End turn minimum radii, R (m)	0.15	0.30	0.30	0.30
Coordinate offset from inlet end, x_i (m)	0	0	0	0
Total current per coil, I (MA turns)	5.872	5.918	6.04	6.0
Filaments through coil width, n (-)	2	2	4	4
Filaments through coil height, m (-)	5	5	8	5

3.1.2 Structural Analysis

The magnetic force containment structure of the preconceptual design magnet was analyzed to verify its ability to withstand forces as determined by the electromagnetic analysis described in Section 3.1.1. The maximum allowable design stresses, listed in Table III, were used as a guide in evaluating the results of the analyses.

The magnetic forces developed by the magnet windings operating at design field strength are shown diagrammatically in Fig. 3. The forces developed per unit length in critical portions of the winding are listed in Table III and are shown diagrammatically in Fig. 4.

The 304LN stainless steel force containment structure around the winding in the plane of the peak on-axis field, which is located approximately 1 m downstream from the inlet-end turn-up of the winding, is shown in Fig. 5. The y-directed force per unit length on one winding bundle in this plane is 776 $\times$ 10^3 kg/m (43.4 $\times$ 10^3 lbs/in) as shown in Fig. 4. The beams are spaced on 20 cm (8 in) centers in the x-direction. The span between tie-rod centerlines is 224 cm (88 in) in the z-direction as indicated in Fig. 5. It is assumed that the beam is uniformly loaded and is point-supported at its ends.

Assumed loading and calculated stresses and deflections are as follows:

Beam:

Total force on one beam (y-dir)	315 tonnes	(693 $\times$ 10^3 lbs)
Distributed load along length	1414 kg/cm	(7.9 $\times$ 10^3 lbs/in)
Bending moment	858 $\times$ 10^3 Nm	(7.6 $\times$ 10^6 in lbs)
Maximum stress, bending	370 MPa	(53.7 kpsi)
Maximum deflection (at center)	0.53 cm	(0.21 in)

Tie-rod:

Force on one tie-rod (y-dir)	157.5 tonnes	(346.5 $\times$ 10^3 lbs)
Tensile stress	338 MPa	(49 kpsi)
Deflection (half-length)	0.28 cm	(0.11 in)

Since the calculated stresses in beam and tie-rod are below the maximum allowable design stresses listed in Table II for Type 304LN stainless steel at 4.5 K, the design is satisfactory. Preliminary calculations show an average stress of 55 kpsi at the thread root area of 6.324 in^2, assuming threads are the 8N series. (See Fig. 5) When detail design is accomplished, the ends of the tie-rods should be examined to ensure that combined stresses in the region of thread roots are below the maximum allowable design stress.

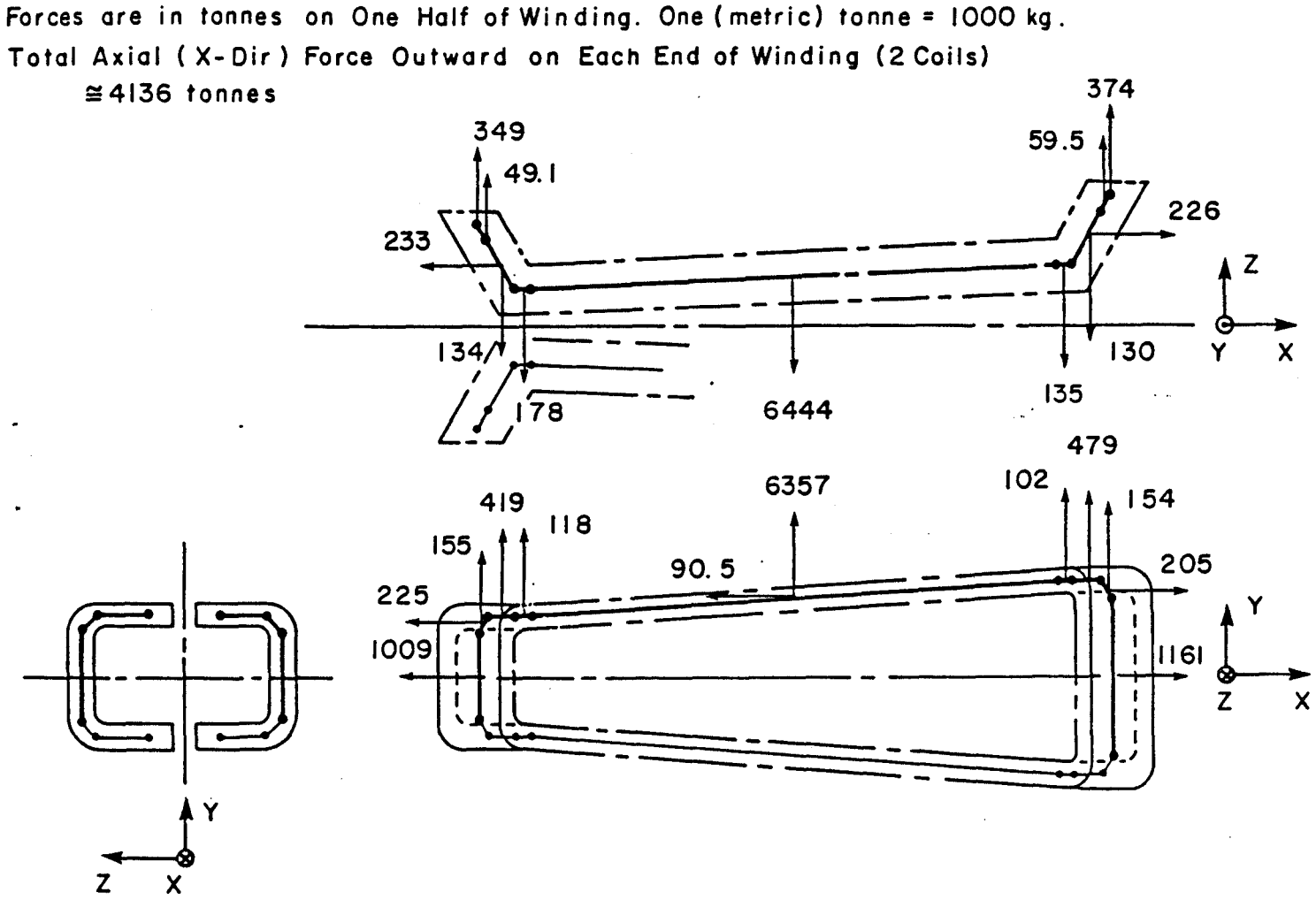

Fig. 3 Diagram of Magnetic Forces Developed by Magnet Winding

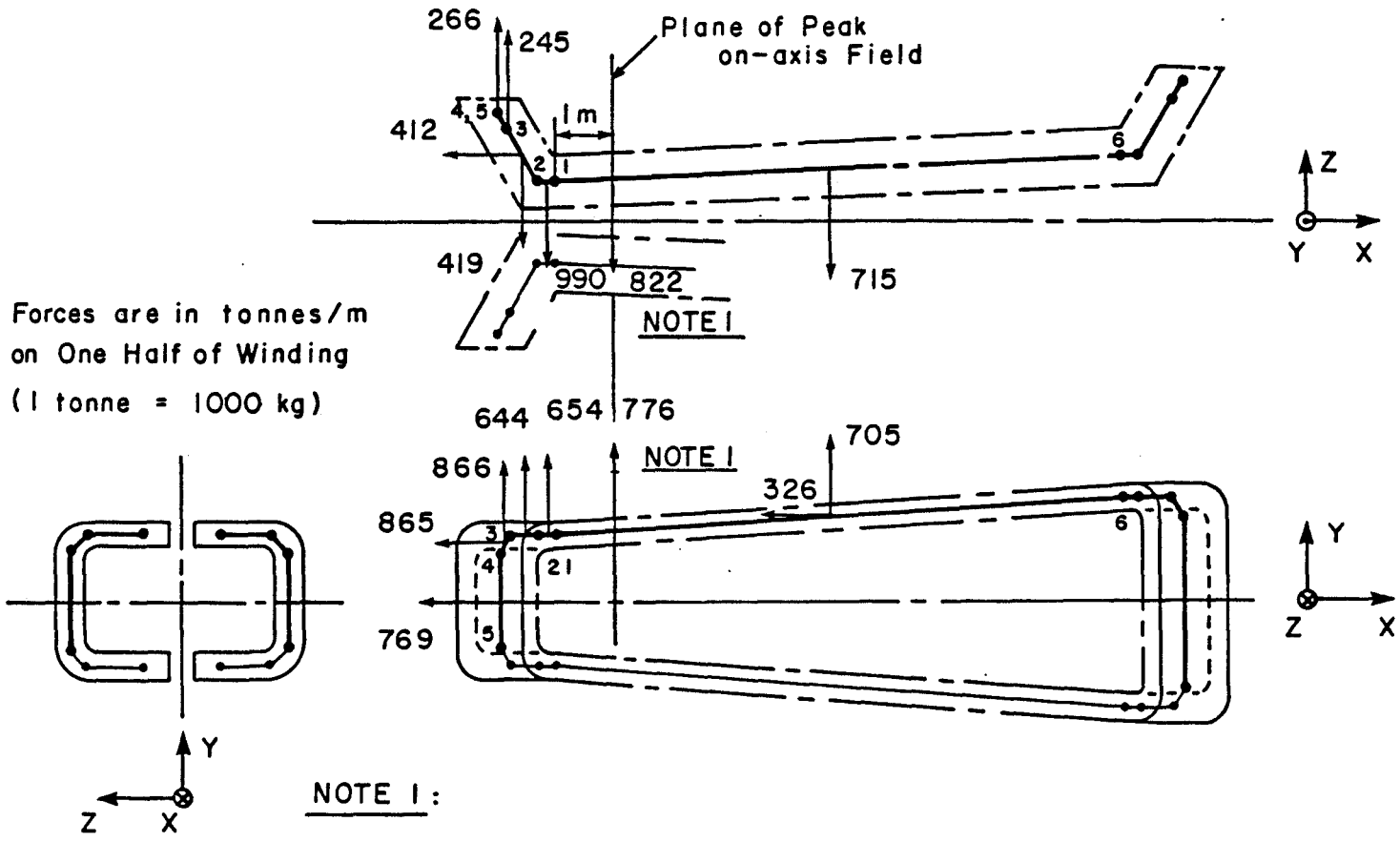

Fig. 4 Diagram of Magnetic Forces per Unit Length Developed by Magnet Winding

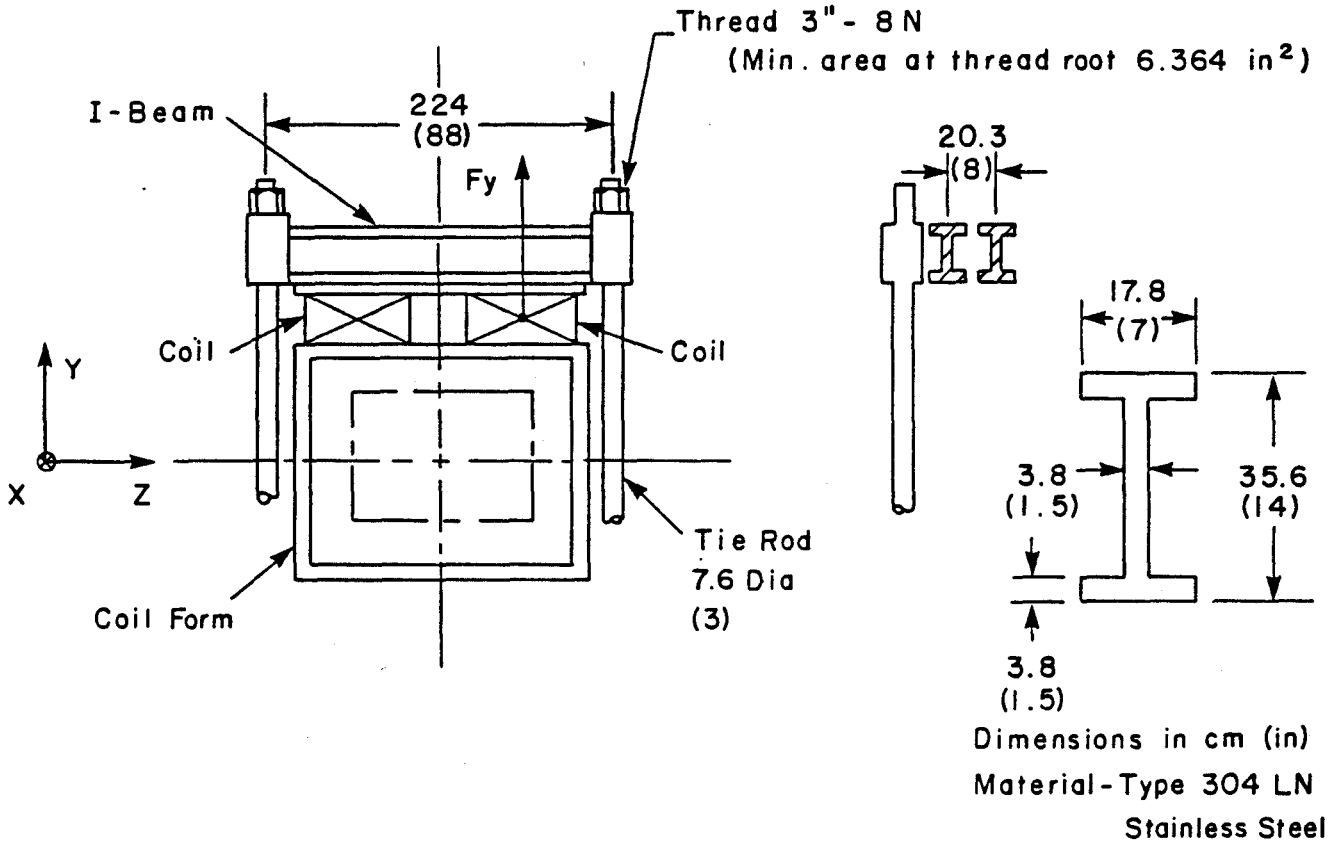

Fig. 5 Sketch of Winding and Force Containment Structure in Plane of Peak On-Axis Field

Table II

MAGNET STRUCTURE MATERIAL PROPERTIES
AND DESIGN STRESSES

Material	Operating Temperature	Assumed Mechanical Properties		Maximum Allowable Design Stress (See Note 1)
		TUS	TYS	
	K	MPa (kpsi)	MPa (kpsi)	MPa (kpsi)
Stainless Steel Type 304LN	300	552 (80)	379 (55)	184 (26.7)
	4.5	1655 (240)	621 (90)	414 (60)

Notes:

1. Maximum allowable design stress is taken as 1/3 TUS or 2/3 TYS, whichever is lower. See Reference 4.
2. TUS = Tensile Ultimate Strength
3. TYS = Tensile Yield Strength
4. 1 Pa = 1 N/m^2

Table III

FORCES PER UNIT LENGTH DEVELOPED BY MAGNET WINDING

Stick*	Projected Length (m)			Force (tonnes)			Force per Unit Length (tonnes/m)		
	x-y	x-z	y-z	x-dir	y-dir	z-dir	x-dir	y-dir	z-dir
1,6	9.01	9.01	0.277	-90.5	6357	-6444	-326	705	-715
1,2	0.18	0.18	0	0	118	-178	0	654	-990
2,3	0.32	0.65	0.565	-233	419	-134	-412	644	-419
3,4	0.20	0.179	0.26	-225	155	49.1	-865	866	245
4,5	1.312	0	1.312	-1009	0	349	-769	0	266

x-dir. force is on y-z plane projection
y-dir. force is on x-z plane projection
z-dir. force is on x-y plane projection

*See Fig. 4 for location of sticks (numbers are given at stick endpoints)

Deflection calculations show that the windings will move away from the coil form during charging, approximately 0.76 cm (0.3 in) at mid-span. However, this amount of motion is acceptable for the type of highly stable winding proposed.

The force containment structure which resists longitudinal (x-direction) magnetic forces is shown in Fig. 6. The total longitudinal force acting outward at each end of the magnet is approximately 4136 tonnes (9.1×10^6 lbs). The major portion of this force is carried by the end plates which transmit it to the structural elements (coil form, cover plates, etc.) running longitudinally from end to end. The cross-sectional areas of structural elements at the plane of peak on-axis field (reference plane) are as follows:

	Area	
Structural Element	(cm^2)	(in^2)
Coil form (6.35 cm thick)	4031	625
Cover plates (3.81 cm thick)	1355	210
Guard vacuum shell (1.27 cm thick)	1761	273
Conductor sheath (0.165 cm thick) (672 conductors)	922	143
Total	8069	1251

Calculated tensile stresses at the reference plane under various assumed conditions are as follows:

	Stress	
Assumed Condition	(MPa)	(kpsi)
Load distributed to all elements	50.1	7.27
Load carried by coil form and guard vacuum shell	69.9	10.13
Load carried by coil form only	100.4	14.56
Load carried by vacuum shell only	229.9	33.33

The coil form, cover plates, and guard vacuum shell are of 304LN stainless steel operating at 4.5 K, for which the maximum allowable stress is 414 MPa (60 kpsi) according to Table II. Based on this analysis, the stress in the longitudinal load-carrying structure is very low (conservative), even when the load is unevenly distributed.

The reason that the calculated stresses due to longitudinal loads are relatively low is that the elements are designed based on other considerations . For example, the coil form is designed with 6.35 cm thick walls to limit y-direction deflection (bending) of the coil-supporting walls of the coil-form cross section under the effect of coil clamping preload to < 0.8 cm, and to limit bending stresses to < 414 MPa (< 60 kpsi).

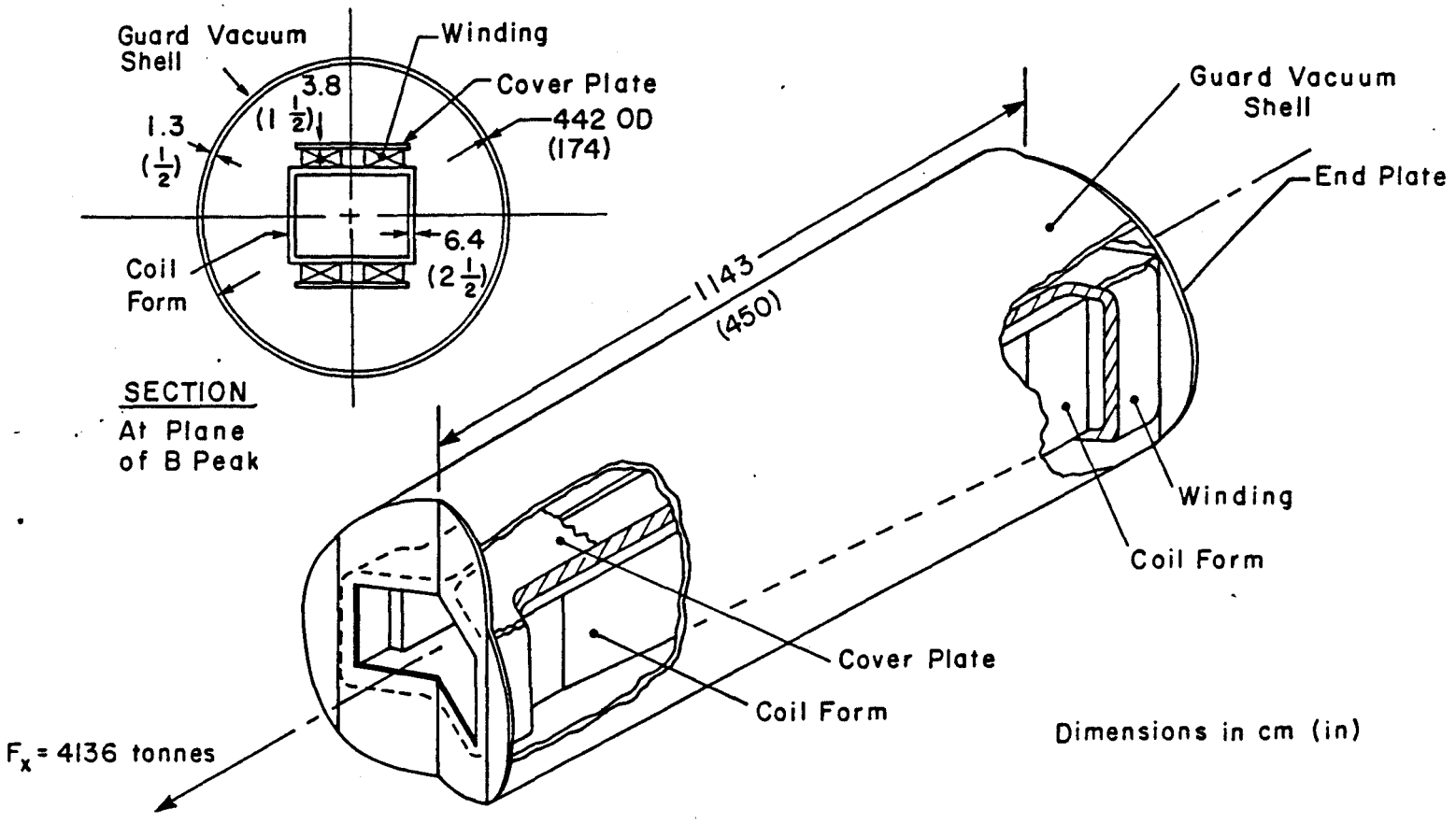

Fig. 6 Sketch of Winding and Longitudinal Force Containment Structure

These preliminary structural analyses indicate that the major elements of the preconceptual design are conservative from a structural standpoint. When the design is carried beyond the preconceptual stage, further structural analysis will be necessary to verify details of the design including fastenings, structural supports in the region of end turns, etc., and to optimize the design for the most economical use of material.

The pressures developed by magnetic forces in the winding bundles against the containment structure in critical areas and the maximum pressures within the bundles were estimated based on data contained in Fig. 4. The results are listed in Table IV. It should be noted that pressures shown are average for the bundle, assuming the insulation between conductors shares loading. If it is assumed that the insulation takes no load, then the pressure on the conductors themselves will be higher by about 27% in the y-direction and 8% in the z-direction. Tests performed on bundles of conductors of the type and size discussed in this report have shown the capability to withstand transverse pressures exceeding 50 MPa (7250 psi).[2]

3.1.3 Thermodynamic Analysis

This section contains a description of the thermodynamic analysis of the magnet and its winding under steady-state operating conditions.

Sources of heating within the winding were determined as follows. Fig. 7 is an electrical and cooling diagram of the winding showing a total of 14 electrical joints (conductor splices) in the two halves of the winding. Based on Westinghouse data[5], the resistance per joint is assumed to be approximately 2×10^{-9} Ω. With a design current of 18 kA, the heating per joint is therefore approximately 0.7 W. This estimated joint loss is subject to change as more experience with ICCS joints is obtained.

Estimated heat leakage and heat generation in the winding and cold (4.5 K) region of the magnet from all sources are listed in Table V. The total equivalent refrigeration at 4.5 K is about 250 W. The magnet is so designed that all conductor splices are located outside of the winding and are immersed in a bath of liquid helium which removes the splice losses. This helium bath also intercepts heat entering through the stack. Therefore, the heat which must be removed from the winding itself consists of thermal radiation of 15 W, conduction of 10 W and flow friction heating of 25 W, for a total of 50 W. The helium coolant flow of 48 g/s, passing through the winding as shown in Fig. 7, removes this heat with a temperature rise of about 0.1 K. The pressure drop in the helium circuit through the windings is estimated to be 0.7 atm. This analysis, necessary in order to establish maximum allowable internal flow resistance of the conductor, is preliminary and will be updated when test data on sample conductors is obtained. *

* It should be noted that in the present design most of the 15 W radiation load will be intercepted by the guard vacuum vessel, thus reducing significantly the winding heat load and the pumping (flow friction) losses. In view of the fact that the guard vacuum vessel is a redundant risk preventative component determined to be prudent because of the lack of long-term (leak free) experience with ICCS (and may thus be eliminated in a future design) full losses have been included in the winding heat load.

Table IV

ESTIMATED PRESSURES DEVELOPED BY MAGNETIC FORCES IN THE WINDING BUNDLES

Location	Direction	Force per Unit Length (Note 1) tonnes/m (10^3lbs/m)	Avg. Press. on Struct. MPa (psi)	Press. Conc. Factor (Note 2) —	Max. Press. in Winding MPa (psi)
Plane of B peak	y	775.9 (1707)	13 (1820)	1.45	18 (2640)
Near Inlet End	z	990 (2178)	31 (4460)	1.2	37 (5350)

Notes: 1. Force on one bundle

2. Pressure Concentration Factor = $\frac{\text{Max. Pressure in Winding}}{\text{Avg. Pressure on Structure}}$ as determined from past experience

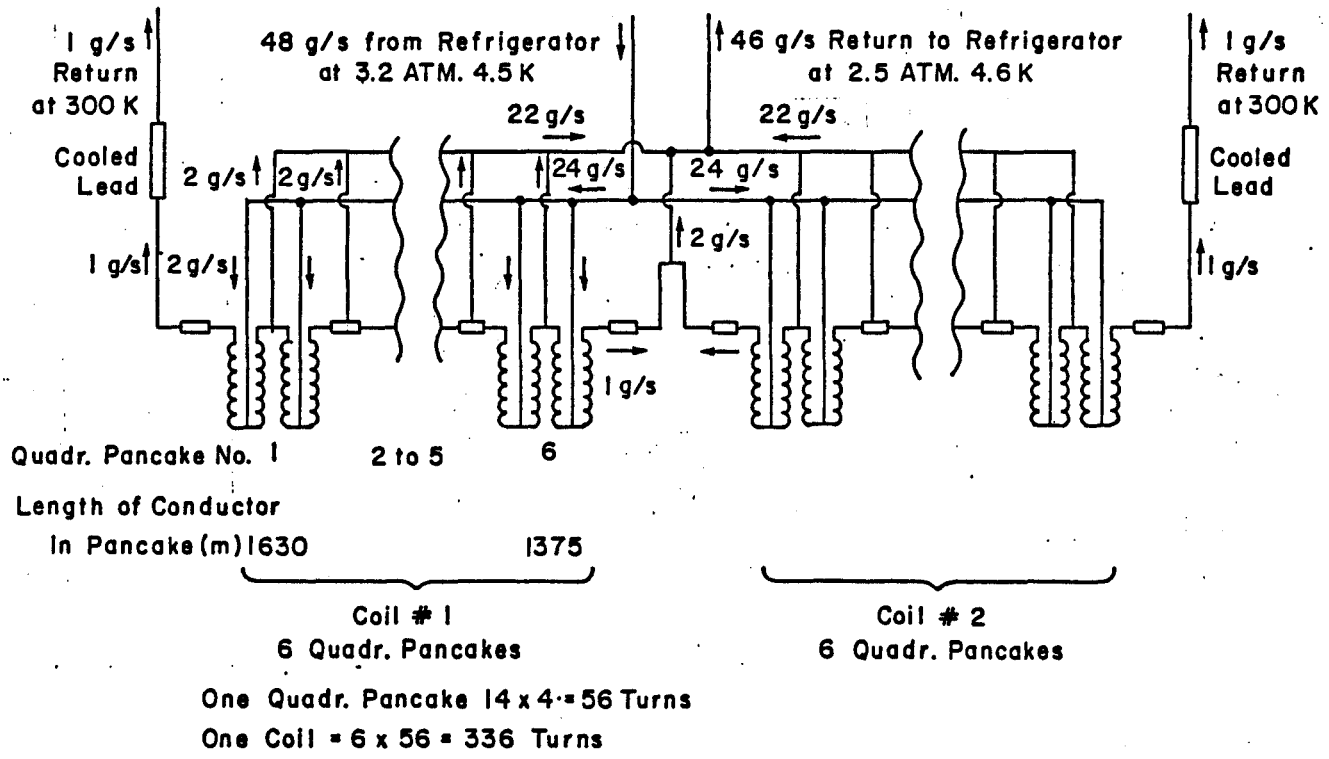

Fig. 7 Electrical and Coolant Flow Diagram, Magnet Winding

Helium refrigeration equipment required for the proposed cryogenic system consists of commercially available components and is not expected to require special development.

Cooldown and warmup subsystems have not been designed and analysed for the retrofit-size magnet, nor has cooldown time been calculated (cooldown time of about 4 weeks would be predicted based on past experience). It is expected that designs for these subsystems developed for other large magnets can be adapted for the retrofit magnet without special development.

Thermodynamic analysis of the conductor itself is described in Section 3.2.

3.1.4 Electrical and Protection System

The electrical and protection (emergency discharge) system, shown in Fig. 8, was analyzed to determine maximum discharge voltage and adiabatic conductor heating during emergency discharge. It was assumed that a number of voltage taps are installed in the winding (at splices or other appropriate locations) and connected to voltage sensing equipment designed to activate the emergency discharge system automatically in the event that a portion of the winding becomes resistive (quenches) due to mechanical or electrical disturbances or other causes. Activation is accomplished by opening the circuit breakers shown in Fig. 8, causing the magnet to discharge through the resistor shown.

In analyzing the emergency discharge system, consideration must be given both to the maximum voltage across the coil and to the maximum temperature to which regions of the conductor rise. Fast discharge results in high voltage across magnet terminals, but is advantageous in limiting the temperature rise in the resistive (quenched) portions of the winding to moderate values. Slow discharge results in lower voltage but higher temperature rise. The actual design will therefore represent a tradeoff between considerations of voltage and temperature rise.

Calculations were made for various discharge time constants (10 to 30 seconds) to determine the resistor resistance value, initial voltage across the winding and maximum temperature rise of the conductor during discharge. It was assumed that the initial current was 18 kA, the initial current density in the conductor copper was 10,500 A/cm^2, and that the conductor heating was adiabatic (no cooling), which is a conservative assumption. Results of this analysis are listed in Table VI. Adiabatic heating of the conductor is also discussed in Section 3.2.3.

A time constant in the range of 10 to 20 s appears suitable for the preconceptual design magnet because, for this range of time constants, voltages are not excessive and conductor temperature remains well below room temperature.

3.2 Conductor Analysis

3.2.1 Structural Analysis of Conductor

The structural characteristics of the conductor were analyzed to determine its ability to withstand tension and transverse loading due to magnetic forces and also internal pressure loading under quench conditions. All three loadings (tension, transverse and internal pressure) cause significant stresses in the conductor of a magnet such as the retrofit MHD magnet and must be considered in establishing conductor design requirements.

Table V

ESTIMATED HEAT LEAKAGE AND HEAT GENERATION IN WINDING AND COLD REGION OF MAGNET

	Heating (W)
Radiation from 80 K thermal shield	15
Conduction through support struts	10
Conduction through stack piping and misc.	10
Conductor splice heating	10
Friction loss due to helium flow in conductor	25
Total	70

Note: In addition to the above, 2 g/s of 4.5 K helium are supplied to cool the power leads, exiting at 300 K. The equivalent refrigeration for the lead cooling is about 180 W at 4.5 K.

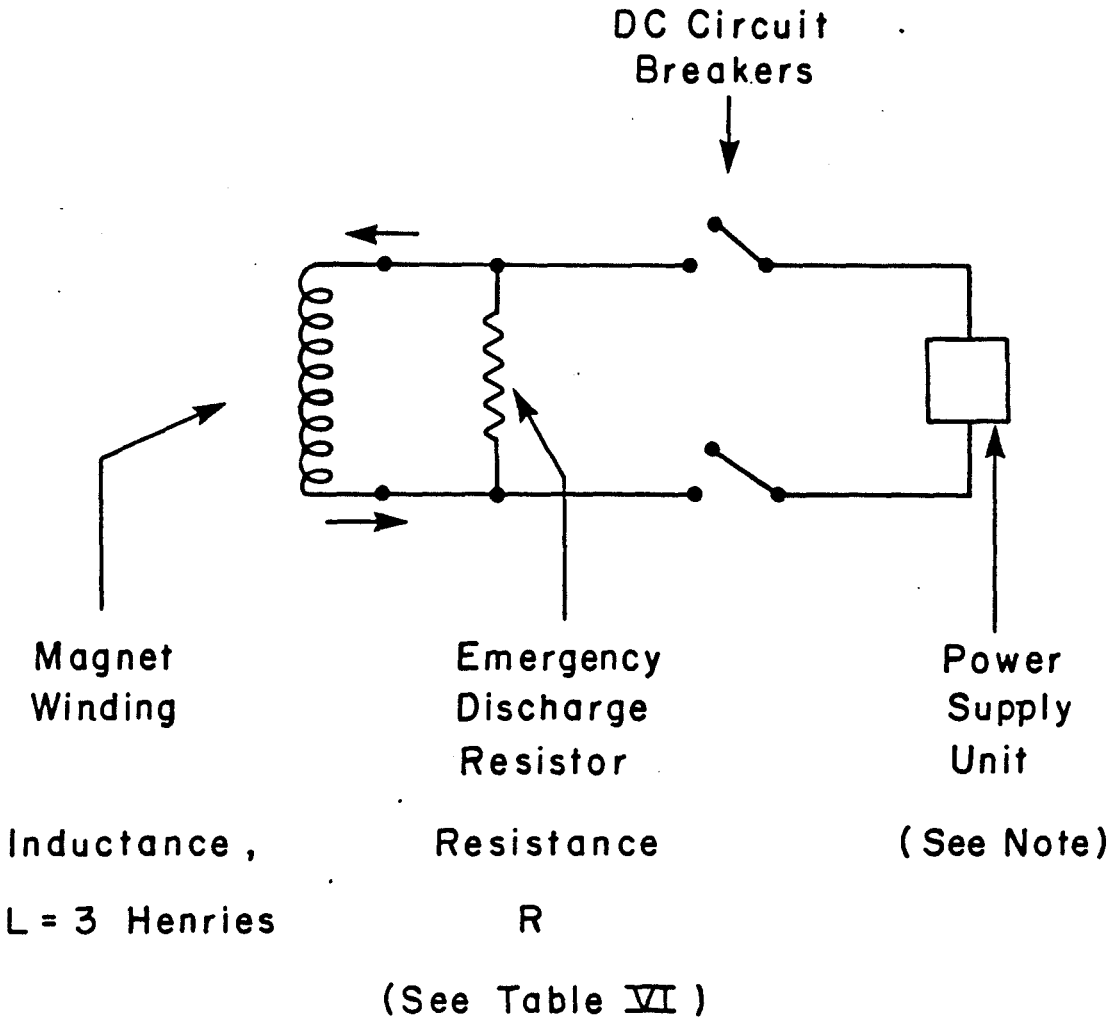

NOTE : Power Supply Max Rating
18,000 A , 30 V

Magnet Charging Time ,
0 to 18,000 A at 30 V = 30 min

Fig. 8 Diagram of Emergency Discharge System.

Table VI

EMERGENCY DISCHARGE VOLTAGE AND CONDUCTOR TEMPERATURE RISE FOR VARIOUS DISCHARGE TIME CONSTANTS

Discharge Time Constant	Discharge Resistor Resistance	Voltage Across Winding	Conductor Temperature Rise (See Note)
(s)	(ohms)	(V)	(K)
10	0.30	5400	95
15	0.20	3600	155
20	0.15	2700	260
30	0.10	1800	600

Note: Assumes initial $J_{Cu} = 10.5 \times 10^3$ A/cm^2

In considering tension loading, it is noted that the conductor in the preconceptual design magnet is supported by structure around the entire outside surface of the winding except for the corners of the end turns, which are unsupported at their outside radii. The result is that hoop tension is applied to the conductors forming the inner portion of these corners, due to Lorentz forces. To verify that the conductor can withstand the hoop tension, a worst case is assumed in which an unsupported turn is exposed to the maximum field (6.9 T) perpendicular to the plane of the end turn. The radius of the inner turn is taken as 0.3 m. With the design current of 18 kA in the conductor, the hoop tension is approximately 3864 kg (8500 lbs). If the effect of a possible quench pressure of 76 MPa (11 kpsi) inside the conductor is added, the total tension in the conductor is approximately 4591 kg (10,100 lbs), resulting in a tension stress in the conductor sheath of about 379 MPa (55 kpsi). Since this is less than 2/3 of the yield strength of the sheath material which is 304 LN at 4.5 K (see Table II), the conductor is satisfactory for the maximum tension load expected. It should be noted that the conductor sheath will actually be in the cold-worked condition and will therefore have a higher yield strength than that given in the table.

Transverse loading of the conductor occurs within the winding where Lorentz forces tend to compress the conductor bundle. Since the preconceptual design magnet does not incorporate any internal support structure (substructure) within the winding, the compressive forces are cumulative and result in relatively high pressures within the winding in high field regions. From the electromagnetic analyses (Section 3.1.1) it is determined that z-directed pressures up to about 37 MPa (5400 psi) will exist in the straight section of the winding near the inlet end.

It is of interest to determine the compressive stress in the conductor sheath, assuming all the pressure load is carried by the sheath. (It is assumed that the cable itself and the insulation do not carry load.) Referring to Fig. 9, plane A-A, the area of sheath material in compression represents 14.6 % of the total area. Therefore, the compressive stress in the sheath is about 225 MPa (37 kpsi). Since this is well below 2/3 of the yield strength of the sheath material (304 LN), the conductor sheath wall thickness is adequate for simple compression loading.

A more comprehensive analysis of this type of conductor under transverse loading is described in Reference 2. Full-scale conductor samples similar to the preconceptual design MHD magnet conductor were compression tested at room temperature and at liquid nitrogen temperature at pressures up to about 152 MPa (22 kpsi). This work, performed as a part of the fusion program, used a conductor which was identical to the proposed MHD magnet conductor except for the following differences:

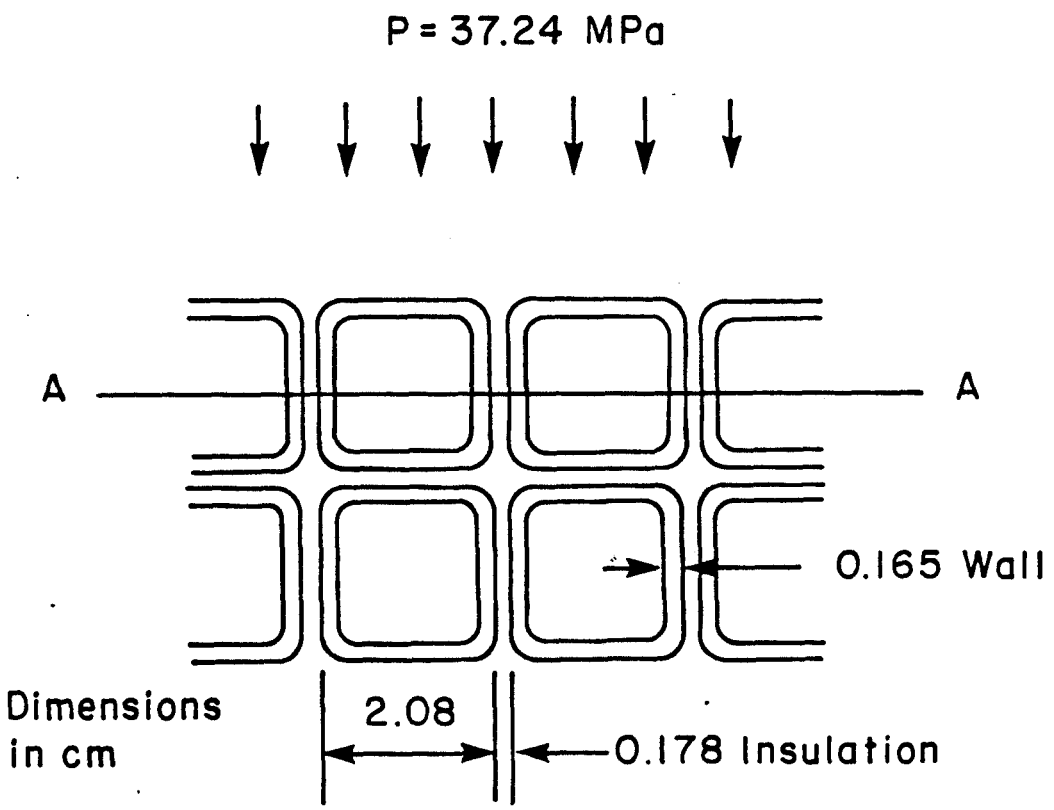

$$\sigma_{sh}/\sigma_o = 2 \times 0.165 / (2.08 + 0.178) = 0.146 \ (14.6\%)$$

Fig. 9 Sketch Showing Cross Section of Conductors in Conductor Bundle

	FUSION PROGRAM CONDUCTOR	MHD CONDUCTOR
Sheath material	JBK-75	304 LN
0.025 mm foil wrap on cable (2 layers)	yes	yes
Superconductor	Nb_3Sn	NbTi
Copper-to-superconductor ratio	1.8 to 1	Range 5 to 1 to 8 to 1

Tests described in Reference 2 were run to determine the load-carrying characteristics of a) the conductor cable itself (top of sheath removed), b) stacks of conduits empty, c) stacks of loose cable-filled conduits, and d) stacks of cable-filled conduits insulated and potted. Conclusions from these tests are listed in Table VII.

The conclusions of Table VII cannot be applied directly to an ICCS for MHD because the latter incorporates a lower strength sheath material and a cable containing a larger proportion of copper, which is expected to result in reduced mechanical properties. However, we can extrapolate from the table to show that the proposed MHD ICCS is adequate for the intended purpose. For example, the maximum acceptable loading of 152 MPa (22 kpsi) given in the table, reduced by the ratio of sheath material yield strengths (see Table 3.1.2-I) becomes about 90 MPa (13 kpsi) for the MHD ICCS. This allowable loading is more than twice the expected actual loading of 37.2 MPa (5400 psi), indicating that the MHD conductor is a conservative design with respect to transverse loading.

With regard to high internal pressure loading such as may occur under quench conditions, tests conducted by Westinghouse and ORNL indicated achievable cryogenic strengths of the order of 1000 atmospheres with conduits similar to those discussed here, presumably of JBK-75 material[2,7]. In addition the following relation has been used in connection with the design of square headers for steam boilers,[2]

$$\sigma = p\omega/2t$$

where σ is the proportional limit (yield) stress of the wall material, p is the internal pressure, w is the width of the rectangular section, and t is the effective wall thickness. Using this expression, maximum design internal pressures are determined as follows (for two assumed values of design stress, σ):

Table VII

CONCLUSIONS FROM EXPLORATORY TESTS OF Nb_3Sn ICCS UNDER TRANSVERSE LOADS[2]

1. A fully wound and potted ICCS coil should be capable of surviving static Lorentz loading greater than 152 MPa (22 kpsi).
2. The presence of corner filler (or potting) undoubtedly is an important factor in achieving that strength.
3. The cable at 32% void fraction appears to support 20% of the pressure applied to the potted and filled conduit.
4. Nonlinear elastic behavior at small loads and (presumably) inelastic behavior at large loads yielded stress-strain curves without a recognizable straight-line region. The steepest slope was approximately 0.5 msi. It occurred at 86.2 MPa (12.5 kpsi) pressure on the stack of filled and potted conduits. A value of 7500 psi was found for the filled and unpotted conduits.
5. The presence of insulation fractures at the corner straight-to-arc transitions indicates high contact pressures at those locations.

Design Stress		Internal Pressure	
(MPa)	(kpsi)	(MPa)	(kpsi)
414	60	78	11.3 (768 atm)
552	80	104	15.1 (1027 atm)

The design stress of 414 MPa (60 kpsi) is taken directly from Table II for 304 LN (annealed) material at 4.5 K. The design stress of 552 MPa (80 kpsi) assumes that the yield strength of the conduit wall has been increased by > 33% through cold work. The higher design stress is 1/3 of the ultimate strength listed in the table.

Pressure testing of samples of ICCS with 304 LN sheath should be performed to finalize the design requirement concerning maximum allowable internal pressure.

3.2.2 Thermodynamic and Pressure Dynamic Analysis of Conductor

Thermodynamic and pressure dynamic analyses of the conductor were performed in parallel with work on the magnet preconceptual design. These analyses are described in this section.

A conductor intended for an early version of the preconceptual magnet design was analyzed early in the program (December, 1984). The major requirements for this conductor are listed in Table VIII together with the assumed dimensions and construction. The calculated characteristics of the conductor, including stability margin, quench temperatures, and quench pressures, are listed in Table IX. These data are based on a NbTi superconductor having a critical current density of 1300 A/mm^2 at 6 T and 4.5 K.

The stability margin is the maximum energy that the ICCS can absorb without quenching when operating at design current, field, and temperature. Calculations of stability margin, including the effect of joule heating, were made with the aid of an existing computer program. The maximum temperatures and pressures with all stored energy dissipated as heating in the conductor and contained helium are based on the assumption that there is no heat exchange with external structure, etc., and no flow of coolant to or from the winding.

From the data listed in Table IX, it appears that the conductor would be satisfactory for this application, except that the ability of the conductor to withstand the quench pressure of 917 atm associated with the length of 600 m between vents would need to be verified by pressure testing. The stability margin of 85 mJ/cm^3 (including the effects of joule heating) is somewhat lower than used for fusion magnets, but is acceptable for the MHD application due to the significantly reduced transient requirements.

Changes in conductor requirements were found to be necessary early in 1985, as a result of further development of the preconceptual magnet design. In particular, it was determined that the maximum field in the winding was higher than originally estimated and that some reduction in average current density and in design current were necessary in order to maintain adequate stability margin. The revised requirements, used as a basis for further conductor analysis, are listed in Table X. Conductor dimensions and construction remain the same as in Table VIII.

Table VIII

REQUIREMENTS, DIMENSIONS AND CONSTRUCTION - CONDUCTOR FOR EARLY VERSION PRECONCEPTUAL DESIGN MAGNET

Requirements:		
Design current	kA	20
Critical current	kA	26.7
Ratio, I/I_c [a]	—	0.75
Maximum field	T	6.0
He coolant temperature	K	4.5
He coolant pressure	atm	2.5
Stored magnetic energy	MJ	321
Conductor total length	km	14.4
Conductor length between vents	m	600
Dimensions and Construction:		
Sheath outside dimensions	cm	2.08×2.08
Sheath corner radius, outside	cm	0.508
Sheath thickness	cm	0.165
Number of strands	—	486
Strand diameter	mm	0.717
Void fraction	—	0.32
Sheath material	—	304 LN
Superconductor composite material	—	NbTi/Cu

[a] The ratio I/I_c is the ratio of the design (operating) current to the critical current of the conductor at the design (operating) temperature and maximum field in the winding. Critical current is the maximum current the conductor can carry without entering the resistive mode.

Table IX

CALCULATED CHARACTERISTICS[a]
CONDUCTOR FOR EARLY VERSION PRECONCEPTUAL DESIGN MAGNET

Copper-to-superconductor ratio	—	8.6
Stability margin based on ΔH^b at constant density	mJ/cm^3	158.1
Stability margin based on ΔH^c at constant density plus joule heating	mJ/cm^3	85
Max. quench pressure, 600 m between vents	atm	917
Max. quench pressure, 300 m between vents	atm	434
Max. temperature of ICCS, all stored energy into heating conductor and contained helium	K	105
Max. pressure, all stored energy into heating conductor and contained helium	atm	439

a) Characteristics are based on NbTi superconductor having a critical current of 1300 A/mm^2 at 6 T and 4.5 K
b) ΔH at constant density is the amount of heat (mJ/cm^3) absorbed by the conductor assuming the density of helium in the conductor remains constant and heat is supplied by an external disturbance only (no resistive heating due to transport current in conductor).
c) ΔH at constant density and joule heating is the amount of heat (mJ/cm^3) absorbed by the conductor assuming helium density remains constant and heat is supplied both by external disturbance and by resistive heating due to transport current.

Table X

REVISED REQUIREMENTS
CONDUCTOR FOR PRECONCEPTUAL DESIGN MAGNET

Design current	kA	15 - 20
Ratio, I/I_c	—	0.75, 0.60
Maximum field	T	6.8 - 6.9
He coolant temperature	K	4.5
He coolant pressure	atm	2.5
Stored magnetic energy	MJ	490
Conductor total length	km	18 ± 3
Conductor length between vents	m	TBD

Three conductors of alternative design were analyzed, based on the revised requirements. The major parameters and calculated characteristics of these conductors are listed in Table XI. For each of these alternatives it was assumed that the stored magnetic energy in the winding was 490 MJ.

The first alternative, a 20 kA conductor with a design current to critical current ratio of 0.75, was found to have a stability margin including joule heating of only 9.5 mJ/cm^3, too low to be acceptable. A variation of this conductor, having a design current to critical current ratio of 0.60, was analyzed to see if a change to the lower current ratio would result in better stability. The stability margin increased only to 13 mJ/cm^3, not a sufficiently high margin to warrant selection of this conductor. Furthermore, the associated reduction in copper would be detrimental to protection of the conductor.

The second alternative, a 17.5 kA conductor (current ratio 0.75) was found to have a stability margin including joule heating of 70.5 mJ/cm^3, which is acceptable for this application. However, the maximum quench pressure of 1107 atm (for the length between vents of 800 m) is somewhat above the range of design pressures discussed in Section 3.2.1 from the standpoint of structural adequacy. Whether this maximum quench pressure is considered acceptable or whether it will be lowered (for example, by reducing length between vents) will depend on the results of future tests including pressure testing of sample conductors. The maximum temperature and pressure reached, with all stored energy transferred into heating of the conductor, are within acceptable limits.

The third alternative, a 15 kA conductor (current ratio 0.75) was found to have a stability margin including joule heating of 106 mJ/cm^3, which is more than adequate for the application. Since this conductor appears to be unnecessarily conservative, it was not analyzed further.

The conductor design selected for incorporation into the revised preconceptual design retrofit magnet was a design falling between alternatives IA and II. It has a design current of 18 kA, a critical current of 24 kA at a maximum field of 6.9 T, a copper-to-superconductor ratio of 7.5 and an estimated stability margin (joule heating included) of 40 mJ/cm^3. This conductor design was selected as the highest current conductor possible, taking into account stability considerations. As for Alternative II, the question of maximum quench pressure must be reviewed in connection with future tests.

3.2.3 Protection

The conductor was analyzed to determine its thermal characteristics with respect to the protection system described in Section 3.1.4. A worst case was assumed, namely an emergency discharge from full design current with only a short section of conductor in the normal state. This section was assumed to be without helium coolant and to be thermally isolated from adjacent winding and structure (i.e., heating was assumed to be adiabatic). Calculations were made to determine the relationship of conductor (adiabatic) temperature rise to design current density in the copper current path and time constant for emergency discharge, assuming exponential current decay. Information contained in Reference 6 was used as a guide. The results of the analysis are shown in Figs. 10 and 11 which contain curves of conductor temperature rise as a function of design current density in the copper for various discharge time constants.

Table XI

MAJOR PARAMETERS AND CALCULATED CHARACTERISTICS
ALTERNATIVE DESIGN CONDUCTORS BASED ON REVISED REQUIREMENTS

		Alternatives			
Major Parameters		I	IA	II	III
Design current	kA	20	20	17.5	15
Critical current	kA	26.7	33.3	23.33	20
Ratio, des. current/crit. current	—	0.75	0.60	0.75	0.75
Field	T	6.9	6.9	6.8	6.8
Superconductor crit. current dens.	A/mm^2	1000	1000	1035	1035
Length between vents	m	700	700	800	800
Calculated Characteristics					
Copper-to-superconductor ratio	—	6.37	4.9	7.72	9.17
Stability margin based on ΔH at const. dens.	mJ/cm^3	123.5	194.8	126	126
Stability margin based on ΔH at const. dens. plus Joule heating	mJ/cm^3	9.5	13	70.5	106
Max. quench pressure	atm	—	—	1107	—
Max. temp. of ICCS, all stored energy into heating conductor and helium	K	—	—	117	—
Max. press., all stored energy into heating conduct. & helium	atm	—	—	489	—

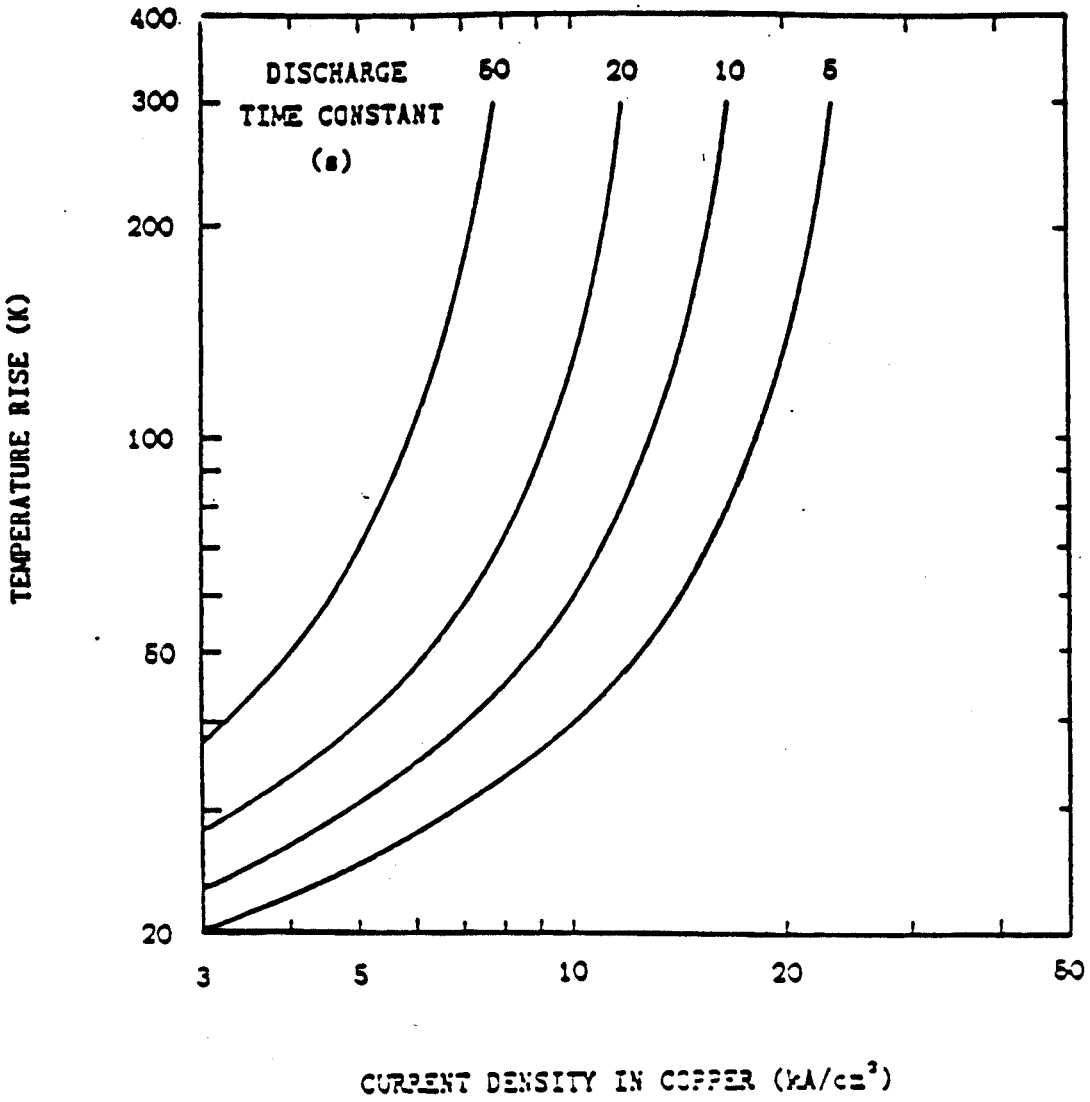

Fig. 10 Curves of Temperature Rise in Conductor vs. Current Density in Copper, Magnetic Field = 0 T

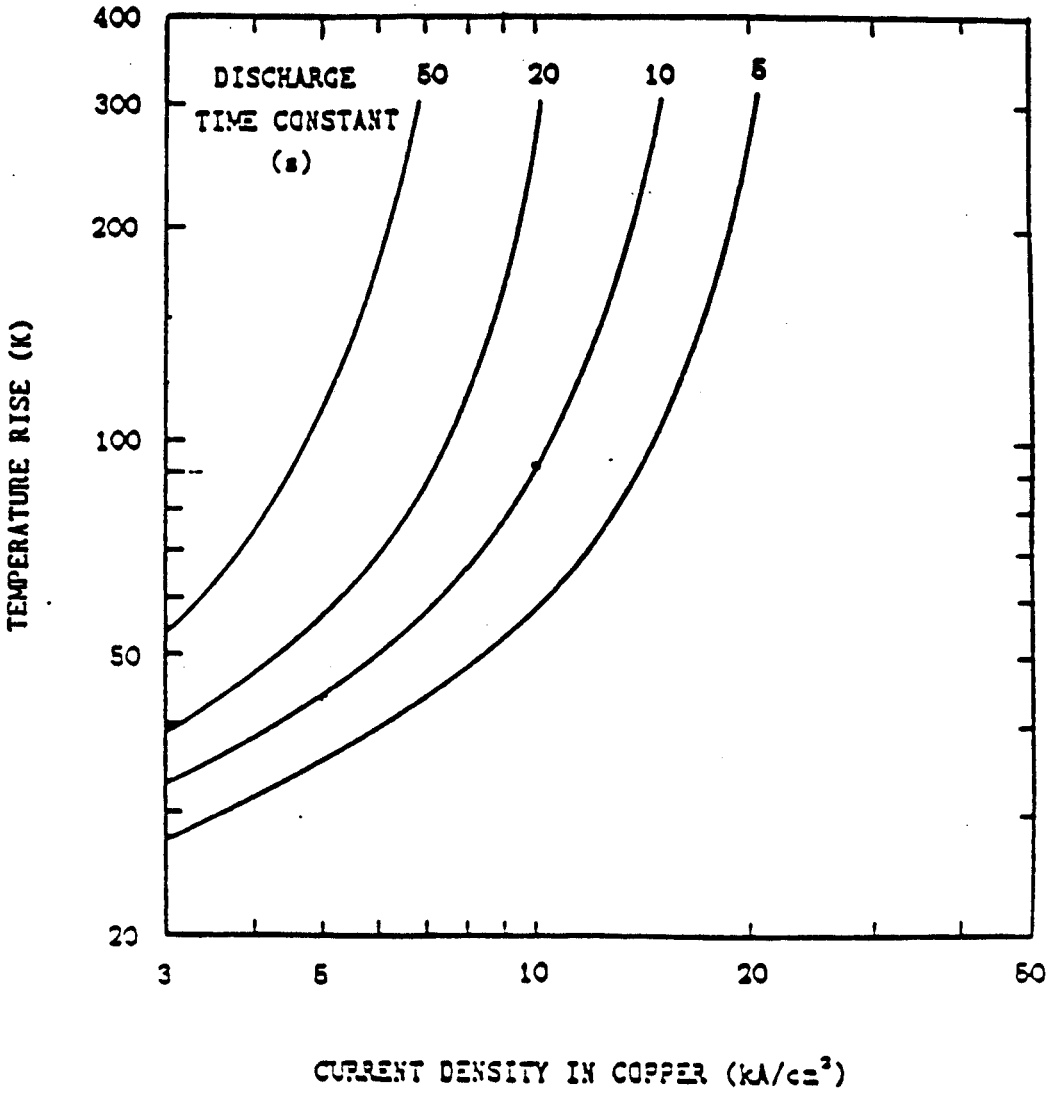

Fig. 11 Curves of Temperature Rise in Conductor vs. Current Density in Copper, Magnetic Field = 6 T

An example of the use of the curves in conductor and system design is given below:

Design current in conductor	18 kA
Magnet inductance	3 H
Discharge resistor resistance	0.3 Ω
Discharge time constant	10 s
Discharge initial voltage	5400 V
Current density in copper, initial	10.5 kA/cm^2
Est. field at conductor, initial	6 T
Final temperature of conductor (from curves Fig. 11)	95 K

If a discharge initial voltage lower than 5400 V is desired, the discharge resistance can be lowered. This will increase the time constant, with a resulting increase in final conductor temperature. In a similar manner, trade-offs can be made among other parameters such as current density in copper, design current, etc.

3.2.4 Definition and Design of Experimental Setup

The definition and design of the experimental setup will be performed in the next period. As anticipated, the analysis performed to date indicates the need for certain special tests, including tests of full-scale conductor samples to determine their ability to withstand internal pressure in addition to tests to determine their stability, quench propagation, and internal pressure dynamics. These tests will be included under Tasks III and IV of this conductor development and test program.

4.0 References

1. Technical Progress Report for Period from January 1, 1985 to June 30, 1985, Develop and Test an ICCS for Large Scale MHD Magnets, Plasma Fusion Center, MIT, Cambridge, MA, November 1985.

2. Becker, H. et al., Structural Behavior of Internally Cooled Cabled Superconductors Under Transverse Load, Plasma Fusion Center, MIT, Cambridge, MA, June 1985. (DOE/ET-15013-151).

3. Design Requirements Definition Report for ICCS for Large Scale MHD Magnets, Plasma Fusion Center, MIT, Cambridge, MA, November 1985.

4. Becker, H., Structural Design Basis for Superconducting Magnets, Draft, MIT/FBNML, 8 February 1980.

5. Phase 2 Final Report to Union Carbide Corp., Nuclear Div., (Contract 22X-31747C) by Westinghouse Electric Corporation, STG Technical Operations Div., Advanced Programs Dept., E. Pittsburgh, PA, March 31, 1980 Vol. II, Part 4, p. 3-813.

6. Course Notes, Magnet Power Supplies and Protection, MIT Summer Session "Superconducting Magnet Design for MHD and Fusion," June 22-26, 1981.

Appendix A Coil Model Generator Computer Program Listing

```
c     MODEL BUILDING PROGRAM FOR TAPERED SADDLE MHD COIL WITH ENDS
c     AT ARBITRARY ANGLES BETWEEN 0 AND 90 DEGREES (NONINCLUSIVE).
      integer p
      real i,len
      open(11,file='REF1',status='new')
c     INPUT FOR PARTICULAR CASE IS AS FOLLOWS:
      len=9.01
      w=0.40
      h=0.50
      ai=0.71
      ao=0.96
      bi=0.08
      bo=0.20
      hi=1.13
      ho=1.37
      ti=45.0
      to=45.0
      r=0.30
      xi=0.0
      i=5.97e6
      n=4
      m=5
c     INPUT COMPLETE
      i=i/(float(n)*float(m))
      ns=16
      nf=2*n*m
      pi=3.14159265359
      ti=ti*pi/180.
      to=to*pi/180.
      hic=bi+h+r*sin(ti)
      hoc=bo+h+r*sin(to)
      if(hi.lt.hic) go to 100
      go to 200
100   continue
      hi=hic
      write(0,1200)
      write(0,1400)
200   continue
      if(ho.lt.hoc) go to 300
      go to 400
300   continue
      ho=hoc
      write(0,1300)
      write(0,1400)
400   continue
      d=1.0-sqrt(2.0-0.5*pi)
```

```
      s=1.0
      p=1000
      write(11,1000) p,ns,nf
c     MODEL UPPER COIL FIRST, THEN NEGATIVE z IMAGE.
500   continue
      do 700 k=1,m
      do 600 j=1,n
      qj=float(j)-0.5
      qk=float(k)-0.5
      wn=w/float(n)
      hm=h/float(m)
      x1=xi
      y1=ai+qj*wn
      z1=s*(bi+qk*hm)
      x2=x1-(h-qk*hm)*tan(ti/2.0)
      x4=x1-(hi-bi)/tan(ti)-h*tan(ti/2.0)+hm*qk/sin(ti)
      x4=x4-wn*qj*cos(ti)
      x3=x4+(1.0-d)*(r+qj*wn)*cos(ti)
      z3=s*(hi-r*sin(ti)+d*(r+qj*wn)*sin(ti))
      y4=ai-r+d*(r+qj*wn)
      z4=s*(hi+qj*wn*sin(ti))
      y5=-y4
      y6=-y1
      x9=xi+len
      y9=-ao-qj*wn
      z9=s*(bo+qk*hm)
      x10=x9+(h-qk*hm)*tan(to/2.0)
      x12=x9+(ho-bo)/tan(to)+h*tan(to/2.0)-hm*qk/sin(to)
      x12=x12+wn*qj*cos(to)
      x11=x12-(1.0-d)*(r+qj*wn)*cos(to)
      z11=s*(ho-r*sin(to)+d*(r+qj*wn)*sin(to))
      y12=-ao+r-d*(r+qj*wn)
      z12=s*(ho+qj*wn*sin(to))
      y13=-y12
      y14=-y9
      p=p+10
      write(11,1100) p,i,x1,y1,z1,x2,y1,z1
      p=p+10
      write(11,1100) p,i,x2,y1,z1,x3,y1,z3
      p=p+10
      write(11,1100) p,i,x3,y1,z3,x4,y4,z4
      p=p+10
      write(11,1100) p,i,x4,y4,z4,x4,y5,z4
      p=p+10
      write(11,1100) p,i,x4,y5,z4,x3,y6,z3
      p=p+10
      write(11,1100) p,i,x3,y6,z3,x2,y6,z1
      p=p+10
      write(11,1100) p,i,x2,y6,z1,x1,y6,z1
      p=p+10
```

```
      write(11,1100) p,i,x1,y6,z1,x9,y9,z9
      p=p+10
      write(11,1100) p,i,x9,y9,z9,x10,y9,z9
      p=p+10
      write(11,1100) p,i,x10,y9,z9,x11,y9,z11
      p=p+10
      write(11,1100) p,i,x11,y9,z11,x12,y12,z12
      p=p+10
      write(11,1100) p,i,x12,y12,z12,x12,y13,z12
      p=p+10
      write(11,1100) p,i,x12,y13,z12,x11,y14,z11
      p=p+10
      write(11,1100) p,i,x11,y14,z11,x10,y14,z9
      p=p+10
      write(11,1100) p,i,x10,y14,z9,x9,y14,z9
      p=p+10
      write(11,1100) p,i,x9,y14,z9,x1,y1,z1
600   continue
700   continue
      if(s.lt.0.0) go to 800
      s=-1.0
      go to 500
800   continue
1000  format(2x,3(i5,2x))
1100  format(2x,i5,2x,1pe10.4,2x,6(0pf10.4))
1200  format(' INPUT VALUE OF hi TOO SMALL.')
1300  format(' INPUT VALUE OF ho TOO SMALL.')
1400  format(' HAS BEEN ADJUSTED TO MINIMUM POSSIBLE VALUE.')
      end
```

Appendix B - List of Symbols

A	amperes
kA	kiloampere (10^3 A)
MA	megampere (10^6 A)
T	tesla (10^6 gauss), magnetic field
m	meter(s)
cm	centimeter(s)
g	gram(s)
kg	kilogram(s) (10^3 g)
K	degrees Kelvin
TUS	tensile ultimate strength
TYS	tensile yield strength
psi	pounds per square inch
kpsi	thousand pounds per square inch
Pa	pascal (1 newton/square meter)
MPa	megapascals (10^6 Pa)
tonne	metric ton (10^3 kg)
in	inch
lb	pound
N	newton
s	second(s)
W	watt(s)
Ω	ohm
R	resistance, electrical
DC	direct current
L	inductance, electrical
V	volt
Cu	copper
J	joule
mJ	millijoule (10^{-3} J)
Nb_3Sn	niobium tin
NbTi	niobium titanium
MHD	magnetohydrodynamic
ICCS	internally cooled, cabled superconductor

σ	stress
p	pressure
atm	atmosphere(s)
I	current, electrical
I_c	critical current
H	enthalpy (thermodynamic)
H	henry, inductance, electrical

Appendix C – Distribution

Mr. Leo E. Makovsky (2 copies)
Technical Project Officer
PM-20, Mail Stop 920-215
Pittsburgh Energy Technology Center
U. S. Department of Energy
P. O. Box 10940
Pittsburgh,PA 15236

Ms. D. G. Sheehan (1 copy)
Contract Specialist
OP-22, Mail Stop 900-L
Pittsburgh Energy Technology Center
U. S. Department of Energy
P. O. Box 10940
Pittsburgh, PA 15236

Mr. Milton Mintz (1 copy)
U.S. Department of Energy
Office of Advanced Energy Conversion
Systems, FE-22, C-119, GTN
Washington, DC 20545

General Counsel for Patents (1 copy)
Chicago Operations Office
9800 South Cass Avenue
Argonne, IL 60439

Mr. Gordon F. Giarrante (1 copy)
Financial Management Division
Chicago Operations Office
U. S. Department of Energy
9800 South Cass Avenue
Argonne, IL 60439

Mr. Paul Gribble
Cost-Price Analyst
OP-22, Mail Stop 900-L
Pittsburgh Energy Technology Center
U. S. Department of Energy
P. O. Box 10940
Pittsburgh, PA 15236

Technical Information Center (2 copies)
U. S. Department of Energy
P. O. Box 62
Oak Ridge, TN 37830

Argonne National Laboratory
9800 S. Cass Avenue
Argonne, IL 60439
Attn: Dr. W. Swift (1 copy)

AVCO Everett Research Lab., Inc.
2385 Revere Beach Parkway
Everett, MA 02149
Attn: Dr. R. Kessler (1 copy)
Mr. S. Petty (1 copy)

Chicago Operations Office
9800 S. Cass Avenue
Attn: Mr. Herbaty, Sr., MHD
Project Manager (1 copy)

Electric Power Research Institute
P.O. Box 10412
3412 Hillview Avenue
Palo Alto, CA 94303
Attn: Mr. A. C. Dolbec, Advanced
Fossil Power Systems (1 copy)
Mr. L. Angelo (1 copy)

STD Corporation
P. O. Box "C"
Arcadia, CA 91006
Attn: Mr. S. Demetriades (1 copy)
Mr. C. Maxwell (1 copy)

Gilbert Associates, Inc.
19644 Club House Road
Suite 820
Gaithersburg, MD 20879
Attn: Dr. W. R. Owens (1 copy)

Mississippi State University
Aerophysics and Aerospace Engineering
P. O. Drawer A/P
Mississippi State, MS 39762
Attn: Dr. W.S. Shepard (1 copy)

Montana State University
Department of Mechanical Engineering
Bozeman, MT 59715
Attn: Dr. R. Rosa (1 copy)

Mountain States Energy, Inc.
P. O. Box 3767
Butte, MT 59702
Attn: Mr. J. Sherick (1 copy)
Mr. G. Staats (1 copy)

Stanford University
Stanford, CA 94305
Attn: Dr. C. Kruger (1 copy)

TRW, Inc.
One Space Park
Redondo Beach, CA 90278
Attn: Dr. A. Solbes (1 copy)
Mr. M. Bauer (1 copy)

U.S. Department of Energy
Idaho Operations Office
785 DOE Place
Idaho Falls, ID 83402
Attn: Mr. G. Vivian (1 copy)

University of Tennessee Space Institute
Tullahoma, TN 37388
Attn: Dr. Susan Wu, Director (1 copy)
Mr. N. R. Johanson (1 copy)

Westinghouse Electric Corporation
Advanced Energy Systems Division
P. O. Box 10864
Pittsburgh, PA 15236
Attn: Mr. G. Parker (1 copy)